Microchimica Acta (2018) 185: 485
https://doi.org/10.1007/s00604-018-3024-y

ORIGINAL PAPER

Biodegradable nanoprobe based on MnO_2 nanoflowers and graphene quantum dots for near infrared fluorescence imaging of glutathione in living cells

Zhi-Ling Song[1] · Xin Dai[1] · Mengru Li[1] · He Teng[1] · Zhen Song[1] · Dexun Xie[2] · Xiliang Luo[1]

Received: 9 July 2018 / Accepted: 24 September 2018 / Published online: 1 October 2018

Abstract
Near infrared (NIR) emitting semiconductor quantum dots can be excellent fluorescent nanoprobes, but the poor biodegradability and potential toxicity limits their application. The authors describe a fluorescent system composed of graphene quantum dots (GQDs) as NIR emitters, and novel MnO_2 nanoflowers as the fluorescence quenchers. The system is shown to be an activatable and biodegradable fluorescent nanoprobe for the "turn-on" detection of intracellular glutathione (GSH). The MnO_2-GQDs nanoprobe is obtained by adsorbing GQDs onto the surface of MnO_2 nanoflowers through electrostatic interaction. This results in the quenching of the NIR fluorescence of the GQDs. In the presence of GSH, the MnO_2-GQDs nanoprobe is degraded and releases Mn^{2+} and free GQDs, respectively. This gives rise to increased fluorescence. The nanoprobe displays high sensitivity to GSH and with a 2.8 μM detection limit. It integrates the advantages of NIR fluorescence and biodegradability, selectivity, biocompatibility and membrane permeability. All this makes it a promising fluorescent nanoprobe for GSH and for cellular imaging of GSH as shown here for the case of MCF-7 cancer cells.

Keywords NIR · GSH · GQD · Bioimaging · Carbon nanoparticle · Manganese dioxide · Biodegradability · Nanoprobe · Redox reaction

Introduction

Glutathione (GSH, L-γ-glutamyl-L-cysteinyl-glycine) is the most abundant cysteine-containing tripeptide thiol (1–10 mM) in cells. It acts as an antioxidant and defender against free radicals, playing a crucial role in the cellular redox homeostasis [1, 2]. Abnormal GSH concentrations have been proved to be related with many diseases, such as cancer, Parkinson's disease, aging, cystic fibrosis and heart problems [3, 4]. Thus, it is considerable to develop applicable methods for monitoring the intracellular GSH levels in living cells.

Fluorometric assays have gained increasing attention for their good reproducibility, high sensitivity, in situ monitoring, real-time spatial image, and non-damaging detection [5–8]. Lots of fluorescent probes based on organic fluorophores have been utilized to sense the intracellular GSH in living cells [9, 10]. However, these fluorescent probes are not applicable for the long-term assays due to such defects as easy photobleaching, poor photostability, low tissue penetration depth and quick renal clearance. NIR fluorescence nanomaterials [11, 12] have attracted significant attention due to their outstanding properties, such as good photostability, deep tissue penetration, good membrane permeability, and reduced autofluorescence, which can effectively avert the renal filtration and help to realize the long-term assays with improved signal-to-noise ratio in living cells and vivo. Quite a few of NIR nanomaterials have been developed for the detection in biological samples. Notably, NIR semiconductor quantum dots (QDs), demonstrating excellent optical properties, have been widely utilized [13–15]. However, due to the concerns of the biodegradability and the

Electronic supplementary material The online version of this article (https://doi.org/10.1007/s00604-018-3024-y) contains supplementary material, which is available to authorized users.

✉ Xiliang Luo
xiliangluo@qust.edu.cn

[1] Key Laboratory of Sensor Analysis of Tumor Marker, Ministry of Education, Shandong Key Laboratory of Biochemical Analysis, Key Laboratory of Analytical Chemistry for Life Science in Universities of Shandong, College of Chemistry and Molecular Engineering, Qingdao University of Science and Technology, Qingdao 266042, China

[2] An Chem-Tech Co., Ltd, Guangzhou 510665, People's Republic of China

potential toxicity of degradation by-products (including heavy metals), the semiconductor QDs have suffered great hindrance in the clinical translation [16, 17]. Therefore, it is imperative to constitute a biocompatible NIR nanosystem for the long-term assays. Alternatively, NIR carbon quantum dots (CQDs) [18–20], including the graphene quantum dots (GQDs) [21] would be the ideal NIR fluorescence nanomaterials, due to the characteristics, such as ultra-small size, non-blinking fluorescence, photostability, aqueous solubility, biocompatibility, photostability and NIR fluorescence emission.

In addition, biodegradable nanoquencher is also a vital component to fabricate the biocompatible "turn-on" NIR nanoprobe. As is well-known, manganese dioxide (MnO_2) nanomaterial is an outstanding quencher [22–24] and can be biodegraded to be Mn^{2+} upon reduction from GSH [25–29]. Zhang group [29] integrated two-photon (TP) mesoporous silica associated with MnO_2 nanosheets, achieving the TP detection of GSH. However, the size and morphology of the above-mentioned MnO_2 were irregular and heterogeneous, which maybe tend to cause the poor reproducibility in vivo analysis. In addition, the used fluorescent nanoprobes were not easy to biodegrade to be the small quantum dots (<5 nm) or chemical molecules, impeding the quick renal clearance. Apparently, it is very significate for facilitating biodegradable "turn-on" NIR nanoprobe of GSH to synthesize uniformed MnO_2 nanomaterials functionalized with NIR GQDs.

We have fabricated activatable and biodegradable NIR fluorescent nanoprobe for intracellular GSH, with the NIR GQDs as the fluorescence reporters and the MnO_2 nanoflowers as the quenchers (Scheme 1). First, the novel MnO_2 nanoflowers were synthesized through the redox reaction of carbon and $KMnO_4$ (Scheme 1a). Such strategy of taking advantage of the carbon nanoparticle as both reactant and template proposed a novel approach toward the growth of uniformed MnO_2 nanostructures. Then, MnO_2 nanoflowers were linked with the NIR GQDs by electrostatic interaction, effectively quenching the NIR fluorescence of GQDs and achieving low background fluorescence for the MnO_2-GQDs nanoprobe. In the presence of GSH, the MnO_2-GQDs nanoprobe was degraded to Mn^{2+} ions and free GQDs, leading to the fluorescence recovery of NIR GQDs. Such nanoprobe showed high sensitivity to target GSH. It also exhibited high selectivity, good biocompatibility and excellent membrane permeability, making it a promising nanoprobe for detecting and imaging GSH in living cells.

Experimental section

Chemicals

N,N-Dimethyldodecylamine, thiophene-3-boronic acid, 4-bromobenzyl bromide, tetrakis (triphenylphosphine) palladium (0) and polyoxyethylenestearyl ether (MW = 4000) were purchased form Alfa Aesar (http://chemicals.thermofisher.cn). Na_2CO_3, $MgSO_4$, CH_2Cl_2, CH_3OH, $FeCl_3$, NaH_2PO_4, Na_2HPO_4, $CHCl_3$, diethyl, EtOH, methanol, L-glutathione (GSH), glucose, $KMnO_4$, N-methylmaleimide (NMM) and α-lipoic acid (LPA) were purchased from Sigma Aldrich Chemical Co (http://www.sigmaaldrich.com). RPMI-1640 medium, penicillin streptomycin solution, and fetal bovine serum were obtained from Hyclone. Cysteine (L-Cys) and homocysteine (Hcy) were purchased from Adamas-beta (http://www.tansoole.com). Tris-HCl buffer solutions (containing Tris, 100 mM NaCl, and 2 mM $MgCl_2$, pH 7.4) and phosphate buffered saline (PBS, containing 0.9% NaCl, pH 7.4) were utilized as working solutions. Human breast cancer cells (MCF-7) were purchased from Guangzhou Cellcook Biotech Co., Ltd., (Guangzhou, China). All other chemicals were of analytical grade and purchased from Sinopharm Chemical Reagent Co., Ltd. (Shanghai, China, https://www.sinoreagent.com). Double-distilled water (resistivity >18 MΩ•cm) obtained from a Milli-Q water purification system was used throughout.

Preparation of MnO_2 Nanoflowers

The MnO_2 Nanoflowers were prepared by hydrothermal treatment with the carbon nanoparticles as templates. First, 0.5 g of glucose was dissolved in 10 mL water, and then the solution was transferred to an autoclave and maintained at 160 °C for

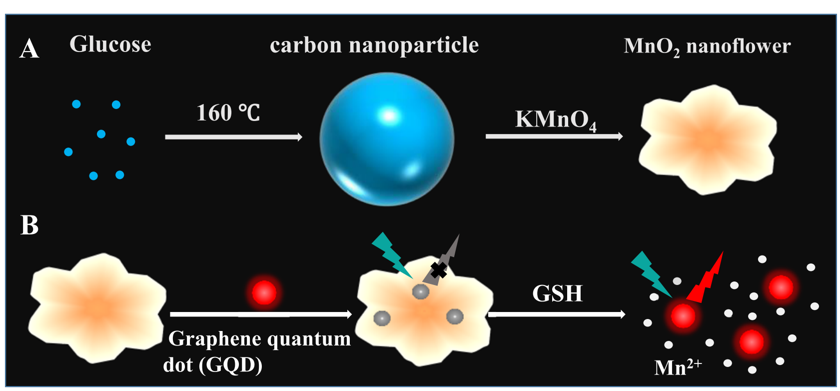

Scheme 1 **a** Schematic illustration of the synthesis of MnO_2 nanoflower. **b** Schematic illustration of the MnO_2-GQDs nanoprobe for the detection of GSH

4 h in oven to synthesize carbon nanoparticles around 100 ± 10 nm. Then, the achieved carbon nanoparticles were collected by centrifugation and washed thoroughly with water for 4 times and then re-dispersed in 5 mL water for further experiments. In order to guarantee the thorough oxidation of carbon nanoparticles, we added rather excess $KMnO_4$ and took long reaction time for a complete reaction between $KMnO_4$ and carbon. 3.5 mL of the above solution was mixed with 11.5 mL of $KMnO_4$ aqueous solution (0.3 M). After being stirred for 15 min, the mixture was added into an autoclave followed by being sealed and maintained at 160 °C for 3 h in oven. After cooling, MnO_2 nanoflowers were collected by centrifugation and washed with water for 2 times. In order to improve the stability and dispersibility of MnO_2 nanoflowers. 1 wt% polyoxyethylenestearyl ether (MW = 4000) was added to the above solution and sonicated for 15 min. Then the mixture solution was washed with water for 2 times to through centrifugation to remove the free polyoxyethylenestearyl ether. Finally, 600 μg mL^{-1} MnO_2 nanoflowers were gained by re-dispersing them in water and stored at 4 °C for further experiment. The concentration of MnO_2 nanoflowers was tested by the Optima 8000 ICP-MS (PerkinElmer), as well as the UV-2450 UV-vis spectrophotometer (Shimadzu).

Synthesis of MnO_2 nanosheets

The process was similar with that of MnO_2 nanoflowers but without the templates of carbon nanoparticles. Briefly, 11.5 mL of 0.03 M $KMnO_4$ solution was added into an autoclave followed by being sealed and maintained at 160 °C for 3 h in oven. After cooling, the MnO_2 nanosheets were collected by centrifugation and washed with water for 4 times. Then MnO_2 nanosheets were re-dispersed in water and stored at 4 °C for further use.

Synthesis of GQDs

The GQDs were synthesized by hydrothermal treatment of polythiophene (PT2) according to previous report by Wang's group [21], in which the sheet-like structures of PT2 turned to be nanodots and the hydrophilic groups spread out to improve the solubility. PT2 shows poor solubility in water, but after the hydrothermal treatment the GQDs product displays commendable solubility in water. Moreover, along with the carbonization of PT2 polymers to water-dispersible nanodots, the GQDs product showed red shift of the fluorescence emission. In brief, 15 mg PT2 was dispersed in 20 mL of NaOH solution (0.5 mM), with a subsequent ultrasonication for about 30 min. The mixture was then removed into a Teflon-lined stainless steel autoclave and reacted at 170 °C for 24 h in oven. After cooling to the room temperature, the reaction product obtained above was filtered through 0.22 μm pore-diameter membranes and then filtrate was dialysed against water. Then, the GQDs were collected by centrifugation. Finally 3 μM GQDs was gained by re-dispersing them in water and stored at 4 °C for further experiment.

Preparation of MnO_2-GQD nanoprobe

0.5 mL MnO_2 (1.2 mg mL^{-1}) were mixed with 0.5 mL GQDs (3 μM) for about 10 min, following by ultrasonic treatment for 5 min. Then MnO_2-GQDs nanoprobe was obtained for the later experiment.

MnO_2-GQDs nanoprobe for the analysis of GSH in vitro

For the analysis of GSH in vitro, 10 μL MnO_2-GQDs solution were mixed with 90 μL GSH in Tris-HCl buffer solutions (20 mM Tris, 100 mM NaCl, and 2 mM $MgCl_2$, pH 7.4) and reacted for 8 min before fluorescent analysis. Finally, the analytical solution was detected through F-7000 fluorescence spectrometer with excitation at 480 nm, and the resulted fluorescence peak intensity at 660 nm was read out and analyzed for the detection of GSH.

Confocal microscopy imaging

Human breast cancer cells (MCF-7) were employed to investigate intracellular GSH levels in cancer cells. MCF-7 cells were purchased from Guangzhou Cellcook Biotech Co., Ltd., (Guangzhou, China). MCF-7 cells were cultured at 37 °C in RPMI 1640 culture medium mixed with 10% premium fetal bovine serum (FBS) and 1% penicillin-streptomycin in a 5% CO_2 environment. In the proliferative period, MCF-7 cells were cultured in a 3 cm optical culture dish with MnO_2-GQDs nanoprobe at 37 °C in a 5% CO_2 atmosphere for 3 h. After discarding the culture medium, the cells were washed three times with 1 mL of Dulbecco's phosphate buffered saline (DPBS, Gibco) (pH 7.4, containing 137.9 mM NaCl, 2.7 mM KCl, 8.1 mM Na_2HPO_4, 1.5 mM KH_2PO_4, 0.9 mM $CaCl_2$ and 0.5 mM $MgCl_2$). And then 1 mL of culture medium was added for subsequently cell imaging. The cellular images were performed with a Leica TCS SP5 inverted confocal microscope using a 20× objective. The excitation source for MnO_2-GQDs nanoprobe was 488 nm, and a 620–700 nm band-pass filter was utilized for fluorescent signal detection.

Results and discussion

Synthesis and characterization of MnO_2 nanoflower and GQDs

The novel MnO_2 nanoflower was synthesized with the prefabricated carbon nanoparticle as templates and followed by hydrothermal treatment. As shown in Scheme 1, the carbon nanoparticle is synthesized by hydrothermal treatment at first and then served as both the template and reductant to fabricate the MnO_2 nanoflower in situ. Notably, the synthesis of MnO_2 nanoflower is based on the redox reaction between carbon and $KMnO_4$ as Eq. 1 [30]. To verify the feasibility of such strategy, Transmission electron microscopy (TEM) and scanning transmission electron microscopy (SEM) was utilized to depict the morphological structure. In Fig. S1A (in the Supporting Information), the generated carbon nanoparticles exhibit highly uniform spherical nanostructure. In Fig. 1, as measured from TEM and SEM images, the MnO_2 nanoflowers demonstrate highly uniformed nanoflower structure and the average size is about 70 ± 9 nm (the number of nanoparticles for calculation $n = 150$). Dynamic light scattering (DLS) characterization further certified the average size (Fig. S1B). Moreover, Raman spectroscopy further certified the successful synthesis of MnO_2 (Fig. S1C), in which the two marked peaks of MnO_2 at around 565 cm^{-1} and 640 cm^{-1} were characterized. Briefly, the carbon nanoparticle confines the growth reaction of MnO_2 specifically to the surface, giving rise to be macroscopically uniform and well-constructed. As a contrast, without the carbon nanoparticles as templates and reactants, the irregular MnO_2 nanosheets were synthesized (Fig. S1D), which certified the importance of carbon nanoparticles for the fabrication of MnO_2 nanoflowers.

$$4MnO_4^{-} + 3C + H_2O \rightarrow 4MnO_2 + CO_3^{2-} + 2HCO_3^{-} \quad (1)$$

NIR GQDs were synthesized by hydrothermal treatment. As shown in Fig. S2, the GQDs product displays commendable solubility and NIR fluorescence in water. TEM (Fig. 1c) was also utilized to depict the morphological structure of GQDs, showing the size distribution around 4 ± 2 nm ($n = 120$). DLS measurement further certified the average size of the GQDs (Fig. S3A). Fig. S3B displays the UV-vis absorption and fluorescence spectrum of the GQDs aqueous solution, demonstrating the broad absorption ranging from 400 to 700 nm, and the NIR emission peak at around 660 nm ($\lambda_{ex} = 480$ nm). The GQDs possessed large Stokes shift and strong NIR fluorescence, which helped to achieve the high-resolution fluorescent imaging with low autofluorescence interference and increase penetration depth in living cells and tissues.

Feasibility of MnO_2-GQDs nanoprobe for the analysis of GSH

To investigate the feasibility of MnO_2-GQDs nanoprobe, the optical properties including UV-vis absorption and fluorescence emission were tested. In Fig. 2a, the GQDs demonstrate strong fluorescence emission peak at 660 nm with excitation at 480 nm, while MnO_2 nanoflowers shows the maximum absorption wavelength at UV region. In fact, MnO_2 nanoflowers has wide absorbance from UV-vis to NIR region. Although the absorbance intensity of low concentration of MnO_2 at NIR region is weak, it can be enhanced obviously with the increase of MnO_2 concentration. MnO_2 nanoflowers possess wide UV-vis absorption spectrum, which is overlapping highly with the fluorescent emission spectrum of GQD. Therefore, the fluorescence of GQDs tends to be effectively quenched by the MnO_2 nanoflowers. The fluorescence emission spectra further verified the reduction of MnO_2 nanoflowers in the presence of GSH. As seen from Fig. 2b, the fluorescence of GQDs is quenched obviously with the formation of MnO_2-GQDs nanoprobe. When GSH was added to the nanoprobe, the fluorescence of GQDs recovered quickly, demonstrating the successful release of free GQDs from MnO_2-GQDs nanoprobe along with the reduction of MnO_2 nanoflowers to Mn^{2+} (Eq. 2) [51]. The telegraphs further declared the efficient degradation of MnO_2, in which the brown MnO_2 solution turned into be colorless in the presence of GSH (Fig. S3C). Moreover, the X-ray photoelectron spectroscopy (XPS) (Fig. S4) were also used. GQDs had obvious O (1 s) and C (1 s) peak, while MnO_2-GQDs showed additional Mn (2p) peak, indicating the corresponding formation of MnO_2-GQDs. The apparent zeta potential measurement was further utilized to testify the feasibility (Fig. S5). GQDs, owning

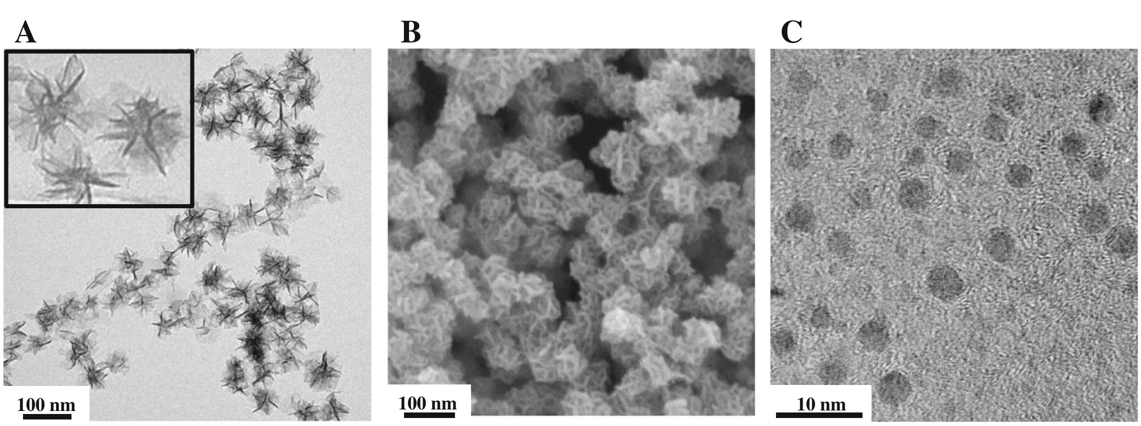

Fig. 1 **a** TEM image of MnO_2 nanoflowers. Inset shows the amplifying image. **b** SEM image of MnO_2 nanoflowers. **c** TEM image of GQDs

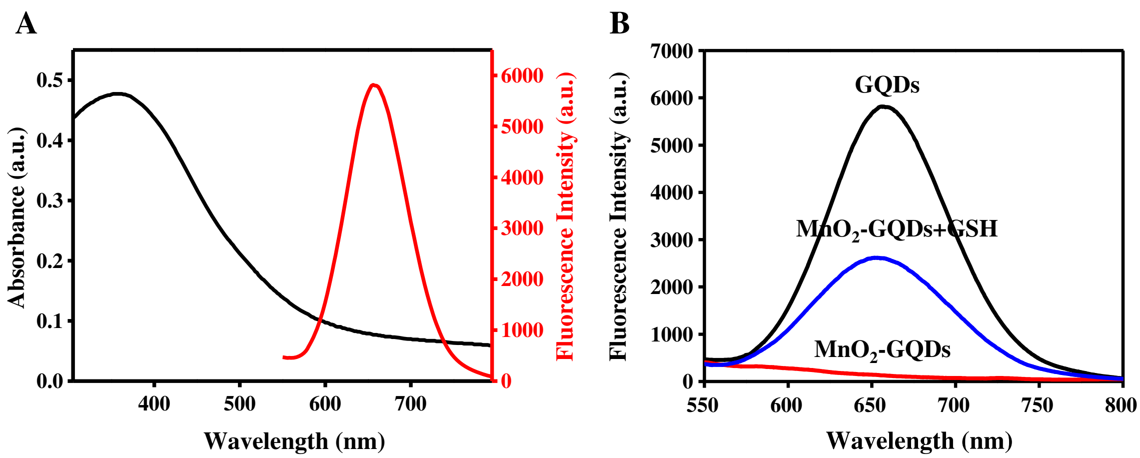

Fig. 2 **a** UV-vis absorption spectrum of MnO_2 nanoflowers (black line) and the fluorescence emission spectrum of the GQDs (red line). **b** Fluorescence emission spectra of the GQDs (black line), MnO_2-GQDs (red line) and MnO_2-GQDs with 1 mM GSH added (blue line) (Excitation wavelength (Ex) at 480 nm; Emission wavelength (Em) at 660 nm)

abundant quaternary amine groups, showed positive apparent zeta potential at around +38 mV, while MnO_2 nanoflowers possessed ample hydroxyl groups and showed negative potential at around −43 mV. Reasonably, MnO_2-GQDs displayed intermediate potential at around +5.52 mV, while in the presence of target GSH, MnO_2-GQDs exhibited positive potential at around +26.6 mV due to the generation of free GQDs. All the measurements demonstrated that MnO_2-GQDs nanoprobe was suitable to detect GSH.

$$MnO_2 + 2GSH + 2H^+ \rightarrow Mn^{2+} + GSSG + 2H_2O \quad (2)$$

Stability of the nanoprobe

It is vital for the ideal fluorescence nanoprobe to detect the target with stable fluorescence performance. In Fig. S6, GQDs display outstanding fluorescence stability even after storage for three months at room temperature. Additionally, the fluorescence stability of the MnO_2-GQDs nanoprobe at different pH was tested (Fig. S7A), which showed almost constant fluorescence intensity from pH 6.8 to 8.4 with the addition of 1 mM GSH, suggesting the super stability in different pH conditions. The fluorescence stability of the nanoprobe in different media was further investigated. In Fig. S7B, the fluorescence intensity of the nanoprobe (with 1 mM GSH added) still shows no obvious changes in different media (H_2O, Tris-HCl and phosphate buffer), demonstrating the commendable stability in different conditions.

Analysis of GSH

We then investigated the analytical capabilities of the MnO_2-GQDs system for GSH activity. In Fig. S8, the quenching efficiency of GQDs with different concentrations of MnO_2 nanoflowers is displayed, and a Stern-Volmer (SV) plot indicates both static and dynamic quenching mechanisms work in the method. [31] Furthermore, when the concentration of MnO_2 was 60 $\mu g\ mL^{-1}$ (GQDs, 0.15 μM), the MnO_2-GQDs platform demonstrated the highest fluorescence sensitivity (Fig. S8). Figure 3 exhibits the fluorescence emission spectra of the MnO_2-GQDs system upon adding different concentrations of target GSH. With the increasing concentration of GSH (from 0 mM to 10 mM) added to the solutions, a gradually increased fluorescence response was observed. The plots of relative fluorescence intensity with different GSH concentrations are shown in Fig. 3b. The fluorescence emission intensity at 660 nm shows a relationship to the concentration of GSH (0 mM to 10 mM). Figure 3b inset shows the line correction between the relative fluorescence intensity of MnO_2-GQDs nanoprobe and the GSH concentration, ranging from 10 to 500 μM. The linear equation is $F/F_0 = 22.72$ [GSH] + 0.7803 (correlation coefficient $R^2 = 0.9971$). The calculated detection limit of GSH was 2.8 μM based on the 3σ rule.

The reaction kinetics were further studied (Fig. S9). Upon the GSH (1 mM) was added to the mixed solution, the fluorescence intensity of the MnO_2-GQDs nanoprobe instantly showed an increase and achieved a stable value in several minutes, which demonstrated the reduction of MnO_2 to Mn^{2+} by GSH leaded to the recovery of fluorescence accompanied with the release of free GQDs from MnO_2 surface. Moreover, with biodegradable performance and rapid response for the target and such nanoprobe would be capable for the bioanalysis and rapid test.

Selectivity

The selectivity is a key factor for the nanoprobe to detect the target in complex practical biological samples. Some reactive species including metal ions and biomolecules

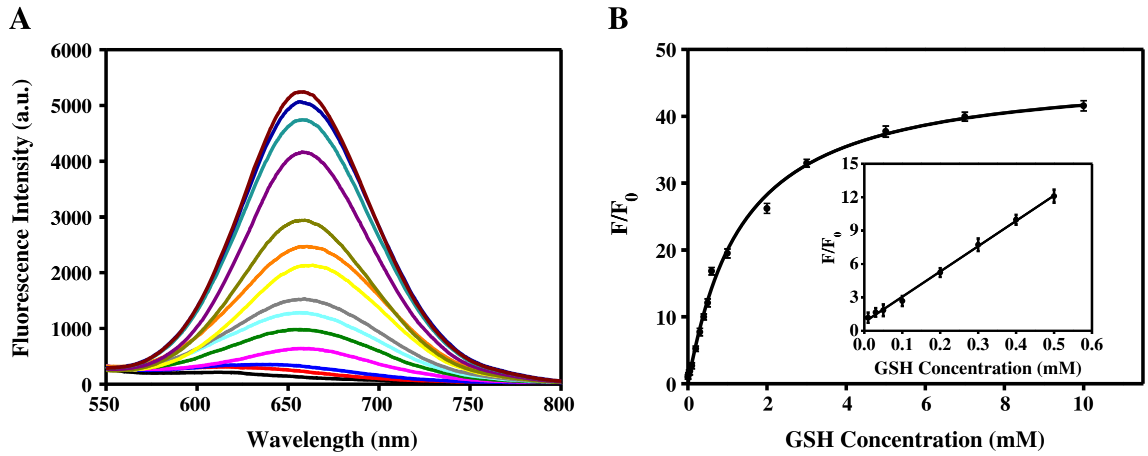

Fig. 3 MnO_2-GQDs fluorescence method for the detection of GSH. **a** Fluorescence-emission spectra of MnO_2-GQDs after incubation with different concentrations of GSH, ranging from 0 to 10 mM. **b** The relationship between F/F_0 and the target concentration. Inset shows the liner responses at low GSH concentrations (F_0 and F are the fluorescence intensity without and with GSH, respectively). Error bars denote the standard deviation ($N = 4$)

generally exist in physiological environment, which would influence the reactive activity of the nanoprobe. To test its specificity for GSH, we challenged the nanoprobe with interfering species containing NaCl, KCl, $CaCl_2$, $MgCl_2$, $MnSO_4$, $NaHCO_3$, PBS, $FeCl_3$, $FeSO_4$, glucose, BSA, Glu, Gys, Gly and GSH (Fig. 4). Markedly higher recovery fluorescence was observed with the target GSH than with the other interfering species, which clearly demonstrated the fine specificity of the MnO_2-GQDs nanoprobe for GSH. The fluorescent response of the nanoprobe for thiol-containing molecules such as L-Cys and Hcy were also measured (Fig. 4). These thiol-containing molecules in the millimolar range can react with the nanoprobes and trigger obvious fluorescent increase in vitro. However, their physiological level (~μM level) is generally much lower than that of GSH (~mM level) in vivo, which indicates that the interfering effects of thiol-containing molecules in cell should be negligible. Therefore, this developed nanoprobe is practical for the detection and imaging of intracellular GSH, which is the amplest thiol-containing molecule in living cells.

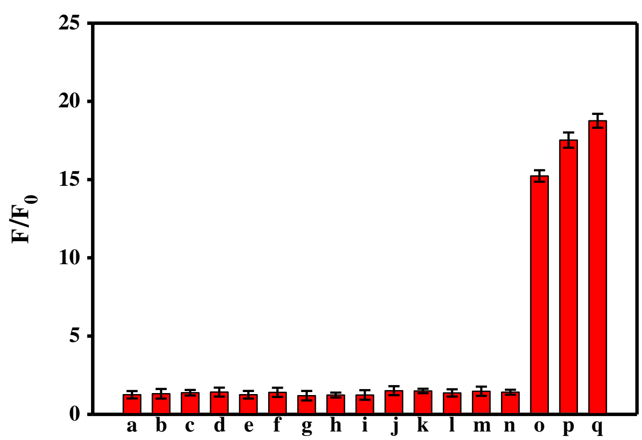

Fig. 4 Selectivity of the MnO_2-GQDs nanoprobes for GSH over other biomolecules (the concentrations of GSH, L-Cys and Hcy is 1 mM, and other agents are 100 mM,respectively). (a, NaCl; b, KCl; c, $CaCl_2$; d, $MgCl_2$; e, $MnSO_4$; f, $NaHCO_3$; g, PBS (pH 7.4); h, $FeCl_3$; I, $FeSO_4$; j, glucose; k, BSA; l, Glu; m, Gys; n, Gly; o, L-cys; p, Hcy; q, GSH). F_0 and F are the fluorescence intensity without and with GSH, respectively. Error bars denote the standard deviation; $N = 4$

Cytotoxicity

Biocompatibility is a key factor for an intracellular nanoprobe system. The cytotoxicity of the MnO_2-GQDs nanoprobe was tested by MTS assay in MCF-7 cells added with different concentrations of nanoprobe (0–80 μg mL^{-1}). As shown in Fig. 5, no obvious cytotoxicity for the cancer cells is observed, which demonstrates that the MnO_2-GQDs nanoprobe possesses good biocompatibility.

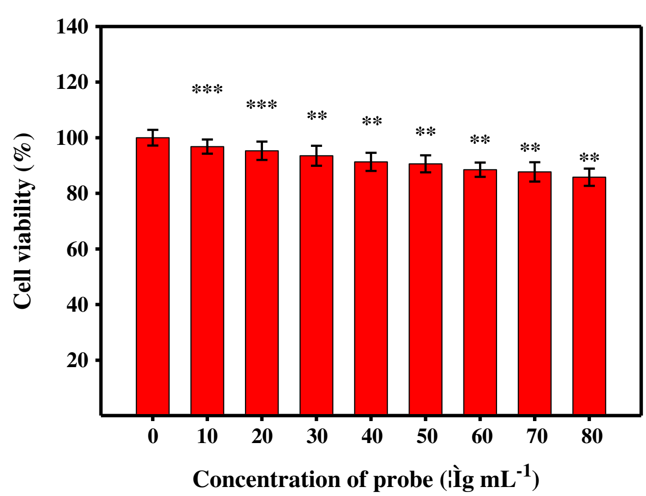

Fig. 5 Cytotoxicity assay of MCF-7 cells treated with MnO_2-GQDs nanoprobes. Error bars denote the standard deviation ($N = 4$). Statistical analysis was calculated through the Student's two-tailed t-test (**$P < 0.01$, ***$P < 0.001$)

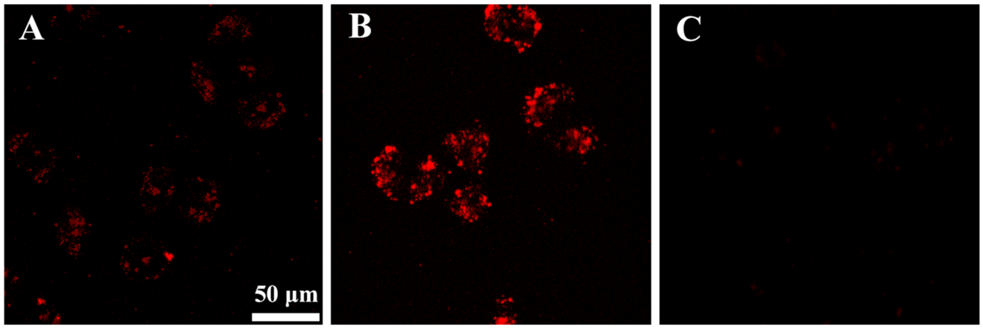

Fig. 6 Confocal microscopy images of GSH detection in live MCF-7 cells. **a** Microscopy image of MCF-7 cells incubated with the MnO_2-GQDs nanoprobe. **b** Microscopy image of MCF-7 cells pretreated with LPA (500 μM) for 24 h followed by incubation with the MnO_2-GQDs nanoprobe. (C) Microscopy image of MCF-7 cells pretreated with NMM (500 μM) for 30 min followed by incubation with the MnO_2-GQDs nanoprobe. (Em:488 nm; collecting wavelength range at 620–700 nm)

Imaging of GSH in living cells

Possessing NIR fluorescence and a large Stokes shift, MnO_2-GQDs nanoprobe can facilitate the high-resolution fluorescent imaging with low auto-fluorescence interference and deep tissue penetration in living cells. Furthermore, endowed with high selectivity, rapid response, good biocompatibility and excellent bio-degradability, MnO_2-GQDs nanoprobe are appropriate for NIR fluorescence imaging GSH in living cells. Then, the capability of such nanoprobe to monitor the intracellular GSH levels in living cells was investigated. With a typical assay, the MnO_2-GQDs nanoprobe was first incubated with MCF-7 cells, and then the sample fluorescence signal was analyzed by exciting with a laser (excitation wavelength at 488 nm) and collecting in the range of 620–700 nm. As shown in Fig. 6a, after incubation with the nanoprobe, MCF-7 cells displayed strong NIR red fluorescence emission, demonstrating the high concentration level of GSH in MCF-7 cancer cells. In addition, it also certified that the unified and homogeneous nanoflower structure endowed the probe with outstanding membrane-permeability. Furthermore, to investigate the capability of the nanoprobe to detect the variation of the GSH concentration level in the living cells, α-lipoic acid (LPA, synthesis enhancer of GSH) and N-methylmaleimide (NMM, scavenger of GSH) were respectively added to the MCF-7 cells in advance. In Fig. 6b, an enhanced fluorescence intensity is observed in the cells pretreated with LPA, while an obvious decreased fluorescence happens to the NMM treated cells, which demonstrates the MnO_2-GQDs nanoprobe is applicable for detecting the intracellular GSH levels with NIR fluorescence imaging. Compared with other fluorescent approaches [23–25, 32, 33], this proposed assay possesses some merits for the application in living cells with deep tissue penetration and reduced autofluorescence (Table S1). However, due to the abundant positive charge and lacking target groups in the surface of the MnO_2-GQDs nanoprobe, our proposed method cannot distinguish different cell lines and has major limitations in the target imaging for the special organelles or cancer cells. We will make great efforts in the target imaging for the special organelles or cells in the future work.

Conclusions

A biodegradable NIR fluorescence nanoprobe (MnO_2-GQDs) for the "turn-on" detection of GSH in living cells was developed, with the NIR GQDs as the fluorescence reporters and the MnO_2 nanoflowers as the fluorescence quenchers. The novel MnO_2 nanoflowers were synthesized by redox reaction with the carbon nanoparticles as both the templates and reactants, exhibiting uniformed nanoscale and morphology. MnO_2-GQDs nanoprobe was established by adsorbing the positively charged NIR GQDs on the surface of negatively charged MnO_2 nanoflowers, and it displayed very low background fluorescence. Upon the activation of GSH, the enhanced NIR fluorescence was observed, because of the efficient degradation of MnO_2-GQDs to Mn^{2+} ions and free GQDs. Such "turn-on" nanoprobe showed high sensitivity and selectivity, good fluorescent stability, excellent biocompatibility and membrane permeability, and it was proved to be a promising nanoprobe for GSH imaging in living cells. Conceivably, this nanoprobe is a novel bioassay platform for targets analysis in-vitro and in-vivo.

Acknowledgements This work was financially supported by the National Natural Science Foundation of China (Grants 21605091 and 21675093), the Natural Science Foundation of Shandong Province of China (Grants ZR2016BB22) and the Taishan Scholar Program of Shandong Province of China (ts20110829).

Compliance with ethical standards The author(s) declare that they have no competing interests

References

1. Liu Z, Zhou X, Miao Y, Hu Y, Kwon N, Wu X, Yoon J (2017) A reversible fluorescent probe for real-time quantitative monitoring of cellular glutathione. Angew Chem Int Ed 56(21):5812–5816
2. Wang Q, Pang H, Dong Y, Chi Y, Fu F (2018) Colorimetric determination of glutathione by using a nanohybrid composed of manganese dioxide and carbon dots. Microchim Acta 185(6):291
3. Qu F, Pei H, Kong R, Zhu S, Xia L (2017) Novel turn-on fluorescent detection of alkaline phosphatase based on green synthesized carbon dots and MnO_2 nanosheets. Talanta 165:136–142
4. Townsend DM, Tew KD, Tapiero H (2003) The importance of glutathione in human disease. Biomed Pharmacother 57(3–4): 145–155
5. Du F, Zeng F, Ming Y, Wu S (2013) Carbon dots-based fluorescent probes for sensitive and selective detection of iodide. Microchim Acta 180(5–6):453–460
6. Zenkl G, Klimant I (2009) Fluorescent acrylamide nanoparticles for boronic acid based sugar sensing from probes to sensors. Microchim Acta 166(1–2):123–131
7. Feng LL, Wu YX, Zhang DL, Hu XX, Zhang J, Wang P, Song ZL, Zhang XB, Tan W (2017) Near infrared graphene quantum dots-based two-photon Nanoprobe for direct bioimaging of endogenous ascorbic acid in living cells. Anal Chem 89(7):4077–4084
8. Heilemann M, Van d LS, Schüttpelz M, Kasper R, Seefeldt B, Mukherjee A, Tinnefeld P, Sauer M (2010) Subdiffraction-resolution fluorescence imaging with conventional fluorescent probes. Angew Chem Int Ed 47(33):6172–6176
9. Zhang H, Liu R, Liu J, Li L, Wang P, Yao SQ, Xu Z, Sun H (2016) A minimalist fluorescent probe for differentiating Cys, Hcy and GSH in live cells. Chem Sci 7(1):256
10. Hinds S, Myrskog S, Levina L, Koleilat G, Yang J, Kelley SO, Sargent EH (2007) NIR-emitting colloidal quantum dots having 26% luminescence quantum yield in buffer solution. J Am Chem Soc 129(23):7218–7219
11. Park J, Dvoracek C, Lee KH, Galloway JF, Bhang HEC, Pomper MG, Searson PC (2011) CuInSe/ZnS core/shell NIR quantum dots for biomedical imaging. Small 7(22):3148–3152
12. Yang T, Tang Y, Liu L, Lv X, Wang Q, Ke H, Deng Y, Yang H, Yang X, Liu G (2017) Size-dependent Ag_2S nanodots for second near-infrared fluorescence /photoacoustics imaging and simultaneous photothermal therapy. ACS Nano 11(2):1848–1857
13. Goswami N, Giri A, Kar S, John R, Xavier PL, Pradeep T, Pal SK (2012) Protein-directed synthesis of NIR-emitting, tunable HgS quantum dots and their applications in metal-ion sensing. Small 8(20):3175–3184
14. Xia C, Meeldijk JD, Gerritsen HC, Donega CDM (2017) Highly luminescent water-dispersible NIR-emitting Wurtzite CuInS2/ZnS Core/Shell colloidal quantum dots. Chem Mater 29(11):4940–4951
15. Xu S, Cui J, Wang L (2016) Recent developments of low-toxicity NIR II quantum dots for sensing and bioimaging. Trac-Trends Anal Chem 80:149–155
16. Ballou B, Lagerholm BC, Ernst LA, Bruchez MP, Waggoner AS (2004) Noninvasive imaging of quantum dots in mice. Bioconjug Chem 15(1):79–86
17. Park JH, Gu L, Maltzahn GV, Ruoslahti E, Bhatia SN, Sailor MJ (2009) Biodegradable luminescent porous silicon nanoparticles for in vivo applications. Nat Mater 8(4):331–336
18. Li H, Liu R, Lian S, Liu Y, Huang H, Kang Z (2013) Near-infrared light controlled photocatalytic activity of carbon quantum dots for highly selective oxidation reaction. Nanoscale 5(8):3289–3297
19. Tao H, Yang K, Ma Z, Wan J, Zhang Y, Kang Z, Liu Z (2011) In vivo NIR fluorescence imaging, biodistribution, and toxicology of photoluminescent carbon dots produced from carbon nanotubes and graphite. Small 8(2):281–290
20. Pei H, Zhu S, Yang M, Kong R, Zheng Y, Qu F (2015) Graphene oxide quantum dots@ silver core–shell nanocrystals as turn-on fluorescent nanoprobe for ultrasensitive detection of prostate specific antigen. Biosens Bioelectron 74:909–914
21. Ge J, Lan M, Zhou B, Liu W, Guo L, Wang H, Jia Q, Niu G, Huang X, Zhou H (2014) A graphene quantum dot photodynamic therapy agent with high singlet oxygen generation. Nat Commun 5:4596
22. Chen J, Huang Z, Meng H, Zhang L, Ji D, Liu J, Yu F, Qu L, Li Z (2018) A facile fluorescence lateral flow biosensor for glutathione detection based on quantum dots-MnO_2 nanocomposites. Sens Actuators B Chem 260:770–777
23. Cai QY, Li J, Ge J, Zhang L, Hu YL, Li ZH, Qu LB (2015) A rapid fluorescence “switch-on” assayforglutathionedetectionby using carbondots–MnO_2 nanocomposites. Biosens Bioelectron 72:31–36
24. Liu Z, Cai X, Lin X, Zheng Y, Wu Y, Chen P, Weng S, Lin L, Lin X (2016) Signal-on fluorescent sensor based on GQDs–MnO_2 composite for glutathione. Anal Methods 8(1):2366–2374
25. Zhang X, Kong R, Tan Q, Qu F, Qu F (2017) A label-free fluorescence turn-on assay for glutathione detection by using MnO_2 nanosheets assisted aggregation-induced emission-silica nanospheres. Talanta 169:1–7
26. Tan Q, Zhang R, Kong R, Kong W, Zhao W, Qu F (2018) Detection of glutathione based on MnO_2 nanosheet-gated mesoporous silica nanoparticles and target induced release of glucose measured with a portable glucose meter. Microchim Acta 185:44–50
27. Yan X, Song Y, Zhu C, Song J, Du D, Su X, Lin Y (2016) Graphene quantum dot-MnO_2 nanosheet-based optical sensing platform: a sensitive fluorescence "turn off-on" nanosensor for glutathione detection and intracellular imaging. ACS Appl Mater Interfaces 8(34): 21990–21996
28. Deng R, Xie X, Vendrell M, Chang YT, Liu X (2011) Intracellular glutathione detection using MnO_2-nanosheet-modified upconversion nanoparticles. J Am Chem Soc 133(50):20168–20171
29. Meng HM, Jin Z, Lv Y, Yang C, Zhang XB, Tan W, Yu RQ (2014) Activatable two-photon fluorescence nanoprobe for bioimaging of glutathione in living cells and tissues. Anal Chem 86(24):12321–12326
30. Liu J, Jiang J, Cheng C, Li H, Zhang J, Gong H, Fan HJ (2011) Co_3O_4 nanowire@MnO_2 ultrathin nanosheet core/shell arrays: a new class of high-performance pseudocapacitive materials. Adv Mater 23(18):2076–2081
31. Zu F, Yan F, Bai Z, Xu J, Wang Y, Huang Y, Zhou X (2017) The quenching of the fluorescence of carbon dots: a review on mechanisms and applications. Microchim Acta 184:1899–1914
32. Wu D, Li G, Chen X, Qiu N, Shi X, Chen G, Sun Z, You J, Wu Y (2017) Fluorometric determination and imaging of glutathione based on a thiol-triggered inner filter effect on the fluorescence of carbon dots. Microchim Acta 184:1923–1931
33. Yang R, Guo X, Jia L, Zhang Y (2017) A fluorescent “on-off-on” assay for selective recognition of cu(II) and glutathione based on modified carbon nanodots, and its application to cellular imaging. Microchim Acta 184:1143–1150